Journal of Energy Storage 83 (2024) 110571

Contents lists available at ScienceDirect

Journal of Energy Storage

journal homepage: www.elsevier.com/locate/est

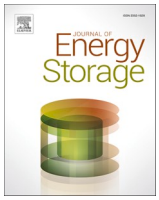

Research papers

Safe and reliable laser ablation assisted disassembly methodology for cylindrical battery cells for post-mortem analysis

Daniel Aeppli [a,*], Jonas Gartmann [a], René Schneider [b], Erwin Hack [a], Sebastian Kretschmer [a], Thi Thu Dieu Nguyen [c], Marcel Held [a]

[a] Transport at Nanoscale Interfaces, Empa - Swiss Federal Laboratories for Materials Science and Technology, Ueberlandstrasse 129, 8600 Dübendorf, Switzerland
[b] Functional Polymers, Empa - Swiss Federal Laboratories for Materials Science and Technology, Ueberlandstrasse 129, 8600 Dübendorf, Switzerland
[c] Battery Electrodes and Cells, Electrochemistry Laboratory, Paul Scherrer Institute, Forschungsstrasse 111, 5232 Villigen PSI, Switzerland

ARTICLE INFO

Keywords:
Cylindrical battery cell
Disassembly
Failure analysis
Degradation
Laser ablation
X-ray

ABSTRACT

Until today, disassembling cylindrical 18650 cells commonly involved using a pipe cutter and pliers, with a risk of short-circuiting and mechanical damage to the electrode materials. This study presents a novel laser ablation assisted disassembly method with X-ray and optical validation for opening cylindrical battery cells without damaging the jelly roll. The objective is to develop a safe, efficient, and reproducible approach for cell disassembly enabling post-mortem analysis of failure mechanisms and investigation of aging effects. X-ray and tube micrometer measurements are used to estimate the cell wall thickness, with good agreement between the two methods. Laser ablation is calibrated to determine the optimal number of laser cycles for achieving the desired ablation depth. In situ temperature measurements are conducted. Various cooling parameters are investigated, maintaining the cell temperature within a safe range of 17 °C to 35 °C during operation. The temperature remains significantly below the reported onset temperature of 57 °C for solid electrolyte interphase (SEI) decomposition. Depth analysis and surface morphology are conducted using confocal microscopy with interferometry and a fully automated digital microscope system. The cells are disassembled within an inert argon atmosphere. Challenges such as redeposition of ablated material and side trench formation are addressed. Overall, this method offers a safe, reproducible and efficient approach for opening cylindrical battery cells. This innovative approach fills a gap in the literature and contributes to advancements in failure analysis and degradation research for the benefit of cell producers, testing laboratories and research institutes.

1. Introduction

Lithium-ion batteries have gained widespread usage in society, with cylindrical cells playing a crucial role. Tesla Motors Inc. highlighted the industrial significance of producing billions of cylindrical type 18650 lithium-ion battery cells annually in 2006 [1]. Since then, the market for cylindrical lithium-ion battery cells, particularly among automotive manufacturers, has witnessed substantial growth [2,3]. The global cylindrical lithium battery pack market is projected to grow at a Compound Annual Growth Rate of 19 % between 2023 and 2028 [4–6]. Cylindrical cells are highly favored among different lithium-ion cell types due to their exceptional mechanical stability, high specific power, and ease of manufacturing [7–10]. Most producers employ steel cases with a Nickel coating for their cylindrical cells, offering high mechanical strength, long life cycle time, and good corrosion resistance [11–13].

Disassembling battery cells is crucial for achieving a circular economy and conserving resources in the increasing use of lithium-ion battery cells [14–21]. Common methods for handling discharged battery cells and modules involve comminution under an inert atmosphere in a shredder process or underwater. However, a laser ablation assisted disassembly process has been proposed for recycling purposes [22,23].

Safe and reliable disassembly processes are particularly relevant for investigating failure analysis and degradation mechanism, especially in low-capacity cells [24–43]. Maintaining an argon atmosphere during disassembly is essential due to the sensitivity of lithium-ion cells to oxygen and moisture [44–48].

Disassembling cylindrical battery cells presents unique challenges compared to pouch and prismatic cells [17,18,49,50]. Various techniques, including dremel tools, pipe cutters, high precision saws, and CNC mill machines, have been employed for disassembling battery cells

* Corresponding author.
E-mail address: daniel.aeppli@empa.ch (D. Aeppli).

https://doi.org/10.1016/j.est.2024.110571
Received 30 August 2023; Received in revised form 19 December 2023; Accepted 11 January 2024
Available online 25 January 2024

in previous studies, each with its own limitations [51–57].

When using dremel tools to eliminate the metallic components near the upper side of the cell and peeling the cell case with pliers, there are potential dangers of short-circuits and mechanical harm to the jelly roll. This method also raises the risk of internal short-circuits due to the presence of metal dust or swarfs. Somerville (2017) noted changes in the solid electrolyte interface (SEI) layer at the negative electrode, caused by dust, particles and other materials during the cutting and electrode removal process [57]. Disassembling 18650-type cylindrical cells without contaminating the sample was not possible. Somerville suggested to overcome this problem by removing only the top cap with a pipe cutter and then peeling the cell can off, e.g. with pliers. Other authors applied this method with the pliers too [53,54]. Since the metal can is thin, peeling the can with pliers could lead to mechanical deformation of the jelly roll, as observed by the authors in previous disassembling tests.

Current techniques often lead to the destruction of internal components or contamination of valuable materials, hindering accurate analysis. The lack of safe and reliable disassembly methods presents hurdles for post-operation material analysis. A critical evaluation of these techniques is vital and is detailed in Section 3.6.

This paper presents a novel laser ablation assisted disassembly method with X-ray and optical validation, offering a solution to avoid damaging cell components, a gap in the existing literature. The proposed method is safe, easy and reproducible, rendering it suitable for both cell producers, testing laboratories, and research institutes.

2. Methodology

2.1. Wall thickness estimation

A commercial cylindrical 18650 cell from Sony, production line US18650 VTC4, with a rated capacity of 2.1 Ah, was used. The steel wall thickness was initially estimated using an X-ray system (Nikon X-Tec XT V 160). Initially, the X-ray beam source, the center of the X-ray detector and the surface of the cell wall are placed within one vertical axis. The cell is moved in order to estimate the wall thickness from the contrast change.

2.2. Laser ablation technique

A custom-built motorized setup, in conjunction with a scanning laser marker (Trotec SpeedMarker 300), was employed. The setup consists of the cylindrical cell positioned on two guiding rolls enclosed in axle bearings (Fig. 1). To prevent slippage, the guiding rolls are coated with soft silicone material. Drive belts connect the guiding rolls to a stepper motor's shaft, ensuring a constant speed. Furthermore, a neodymium magnet is used to securely hold the cell in place on its positive terminal.

To safely disassemble cylindrical battery cells and achieve the desired laser ablation depths of 150 to 200 µm, a wobbling laser line with a length of 200 µm is applied parallel to the main axis of the cell, while the cell undergoes constant rotation. The optimized laser parameter procedure results in the formation of side trenches, but their impact on the final laser trench is minimal. A comprehensive analysis and visual representation of this phenomenon can be found in Sections 3.2 (Fig. 4) and 3.3 (Fig. 5).

The determination of the optimal number of laser cycles necessary to create the final laser trench depends on material parameters, including the characteristics of the cell wall and the laser system employed. Initially, a few laser cycles are applied, and then the evaluation process begins to determine the optimal number of laser cycles needed. This evaluation is carried out using calibration lines, as described in detail below.

Three calibration line series were implemented, positioned near the bottom side (Fig. 1, 1a), in the center of the cell case (Fig. 1, 1b), and close to the top side (Fig. 1, 1c). Laser calibration lines covering a range of 40,000 to 200,000 laser cycles were employed with a line spacing of 300 µm, Fig. 2(a). The reference length for estimating the wall thickness was determined by measuring the distance between the marking lines near points A and B (as shown in Fig. 2(a)), which measured 1800 µm. A simplified linear least square regression analysis with zero intercept was performed on each calibration line series using a graphical approach (Fig. 2(a)). The linearization process involved utilizing the depth of the midpoint of the laser trench. To ensure accuracy and consistency, the X-ray image in Fig. 2(a) was flipped horizontally and vertically to eliminate any potential inaccuracies caused by variations in viewing angles on the screen. The consistent results obtained from all four images, indicating the same estimated ablated depth, demonstrate the robustness of this method.

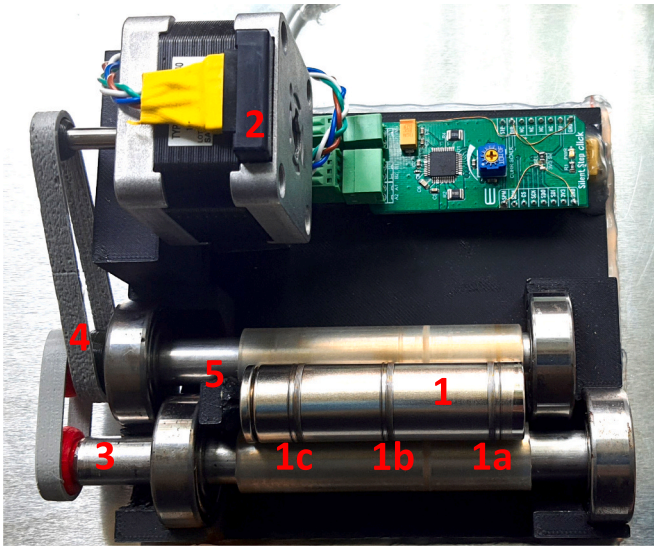

Fig. 1. Setup. 1 Battery cell with calibration line series and final laser trenches at positions 1a, 1b and 1c.
2 Motor, 3 Guiding rolls, 4 Drive belts, 5 Magnet.

Based on the authors' extensive experience in disassembling cylindrical cells, it is suggested to maintain a residual wall thickness of 30 to 40 µm to ensure breakability of the cell wall while preserving mechanical stability. To provide an additional safety margin, a conservative value of 40 µm is adopted in this study. This recommended residual wall thickness ensures effective disassembly while minimizing the risk of structural integrity issues. By extrapolating the slope, the number of laser required to ablate the entire wall thickness less 40 µm as a safety margin were calculated.

The calculated number of laser cycles for the final laser trench was applied in close proximity to the calibration series. Specifically, the marking line of the final laser trench (C) was 700 µm distant from the marking line of the calibration series (B), as shown in Fig. 2. The safety margin from the final laser trench is clearly evident from the results shown in Fig. 2(b). The impact of the side trenches on the final laser trench is negligible. The distance between the marking lines near points C and D, which measured 600 µm, as illustrated in Fig. 2(b), was used as the reference length for determining the final laser trench ablation depth.

Proximity of the cell to the beam source can result in higher cone beam aspect distortion in the cone beam geometry during radiography. This distortion can impact the interpretation of the laser calibration line's actual ablation depth. Positioning the cell closer to the detector reduces the distortion but sacrifices image sharpness due to lower magnification. To ensure accurate X-ray measurements, it is important to position the cell at a sufficient distance from the X-ray beam source—25.5 mm for the calibration lines (Fig. 2(a)) and 16.7 mm for the final laser trench (Fig. 2(b)). The images were processed using FIJI

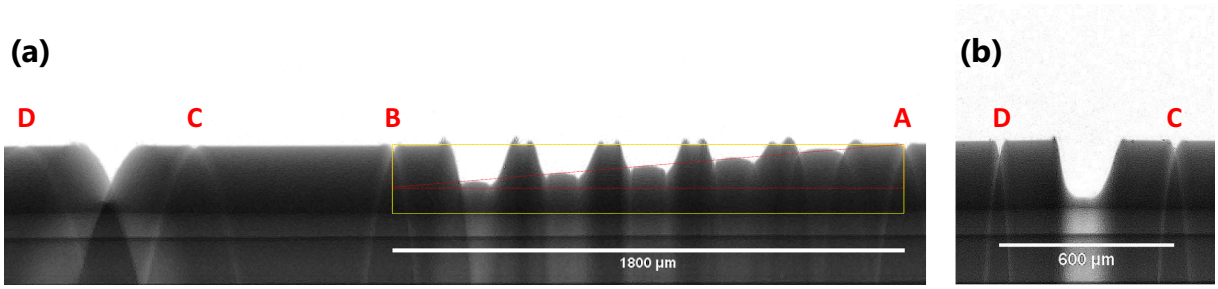

Fig. 2. X-ray image of the calibration lines in increments of 40,000 laser cycles and final laser trench (Fig. 1, 1c) with marking lines A, B, C and D. (a) Calibration lines. (b) Final laser trench close to the top side.

ImageJ software (v. 1.53q; with CLAHE plugin v. 1.4.1) to enhance sharpness and local contrast.

2.3. Disassembly technique

After laser ablation, the cells with a remaining wall thickness of 40 µm were disassembled inside an argon-filled glovebox (MBRAUN LABmaster Pro SP) using two water pump pliers (HAZET 760). Plastic materials covered the water pump pliers for a secure grip. The disassembly process involved a counter-clockwise rotation in close proximity to the laser lines (Fig. 3). Minimal force was required to successfully break the laser trenches, ensuring no damage to the jelly roll. Separation of the jelly roll from the cell case was facilitated by a rubber plug from a piston syringe.

After removal, the jelly roll can be analyzed directly within the glovebox. Alternatively, it can be covered with insulating Parafilm® to prevent any potential short-circuits during storage and transport. To safeguard against moisture and oxygen, it is also suggested to place the Parafilm®-covered jelly rolls inside aluminum bottles or barrier foil locking pouch bags.

3. Results and discussion

3.1. Application to different cells of the same type and production lot

The methodology employed in this study was validated using four different types of cylindrical 18650 cells. These cells are sourced from different manufacturers, including APR, Sony, Samsung, and Yinlong. In this Section 3, exclusively cells of Sony's US18650VTC4 production line are utilized.

The cell wall thickness is determined using a tube micrometer (TESA Brütsch/Rüegger, AL ISOMASTER), yielding 231 ± 1 µm (1 standard deviation, 1 SD, 8 cells). X-ray measurements (Fig. 2b) yielded a wall thickness of 229 ± 1 µm (1 SD, 8 cells). The two methods are consistent within 2 SDs.

The cell wall thickness of the cell is measured using a tube

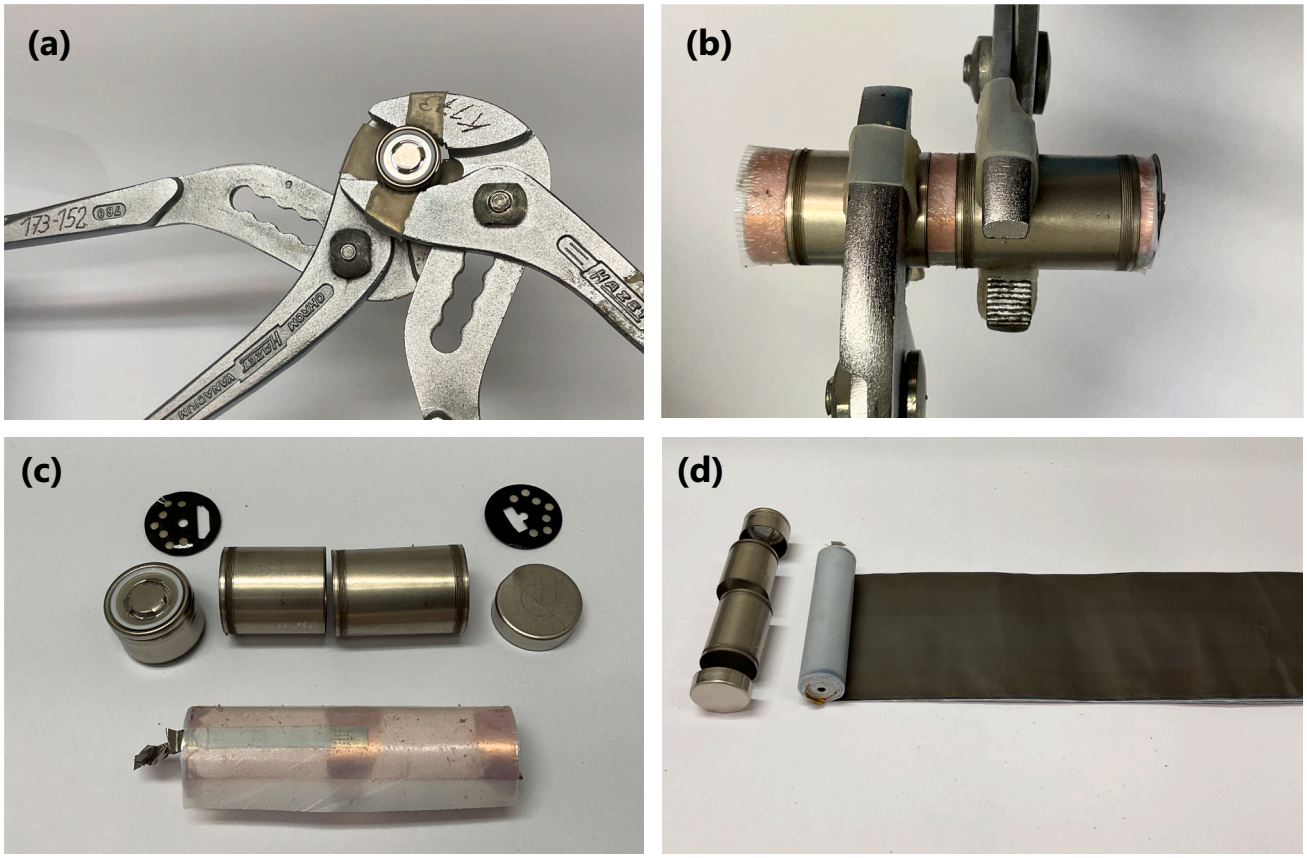

Fig. 3. Disassembly procedure within the glovebox. (a) Orthogonally placed water pump pliers. (b) Cell opened. (c) Cell disassembled. (d) Jelly roll unrolled.

micrometer at three different positions, each at 4 rotational orientations. Near the bottom side (Fig. 1, line 1a), the thickness is 232 ± 1 μm. Near the center of the cell case (Fig. 1, line 1b), the thickness is 231 ± 1 μm. Near the top side (Fig. 1, line 1c), the thickness is 230 ± 1 μm. These measurements show that the cell wall thickness remains almost constant along the length of the cell within 2 SDs. However, it is important for cells of other cell manufacturers to use the proposed method with three positions in case their wall thickness varies along the length of the cell.

Based on the extrapolation of the calibration lines, the required ablation depth is determined to be 189 μm, which is obtained by subtracting 40 μm safety margin from the X-ray estimated wall thickness of 229 μm. It is calculated that 300,000 laser cycles are necessary to achieve the desired ablation depth. The depth of the laser-ablated lines on the tested cell is estimated to be 188 ± 4 μm (1 SD, 8 cells) using X-ray analysis and 188 ± 5 μm using confocal microscopy (Leica DCM8). These measurements closely align with the extrapolated anticipated ablation depth of 189 μm.

The cell diameter is measured using an electrical caliper (TOOLCRAFT S/N: 220–150–158-1) was 18.01 ± 0.02 mm close to the bottom side of the cell and 18.05 ± 0.02 mm close to the top side of the cell (1 SD, 4 measurements). Measurements are taken at orthogonal positions to assess cell non-circularity. A difference of 20 μm in focus height can result in a 2 μm variation in ablation depth, necessitating the calibration lines to be applied approximately 1 mm away from the final laser trench. The 2 μm difference resulting from any imperfections in the cell's roundness is accounted for within the 40 μm safety margin.

3.2. Optical microscopy for determining the depth of the final laser trenches

To evaluate the surface morphology of the laser trenches, a nondestructive, confocal 3D Optical Surface Metrology System (DCM8) with a Leica EPI 50× objective is used. Data analysis is performed with Leica Map 7.4 software to yield the depth and 3-D images of the laser trenches. For comparison, a digital microscope (Keyence VHX-7000) with a 200× objective and VHX software (v. 1.4.23.17) is used.

A least squares linear regression analysis is performed on the measurement points, with the intercept forced through zero. The linearization process involved utilizing the depth of the midpoint of the laser trench. The results are shown in Fig. 4.

The results yield slopes of 6.154×10^{-4} μm/laser cycle for Ablation X-ray (Nikon), 6.136×10^{-4} μm/laser cycle for Ablation Optical (Leica) and 6.157×10^{-4} μm/laser cycle for Ablation Optical (Keyence). Utilizing the extrapolated method of 300,000 laser cycles, the estimated laser depths are 185 μm (X-ray), 184 μm (Optical Leica), and 185 μm (Optical Keyence).

The coefficient of determination (R^2), including the origin (0,0), is 0.996 for ablation X-ray (Nikon) and for ablation Optical (Keyence) and 0.995 for ablation Optical (Leica).

The additional depth of the side trenches is non-proportional to the amount of applied laser cycles and becomes neglectable for the final laser trench as illustrated in Fig. 5.

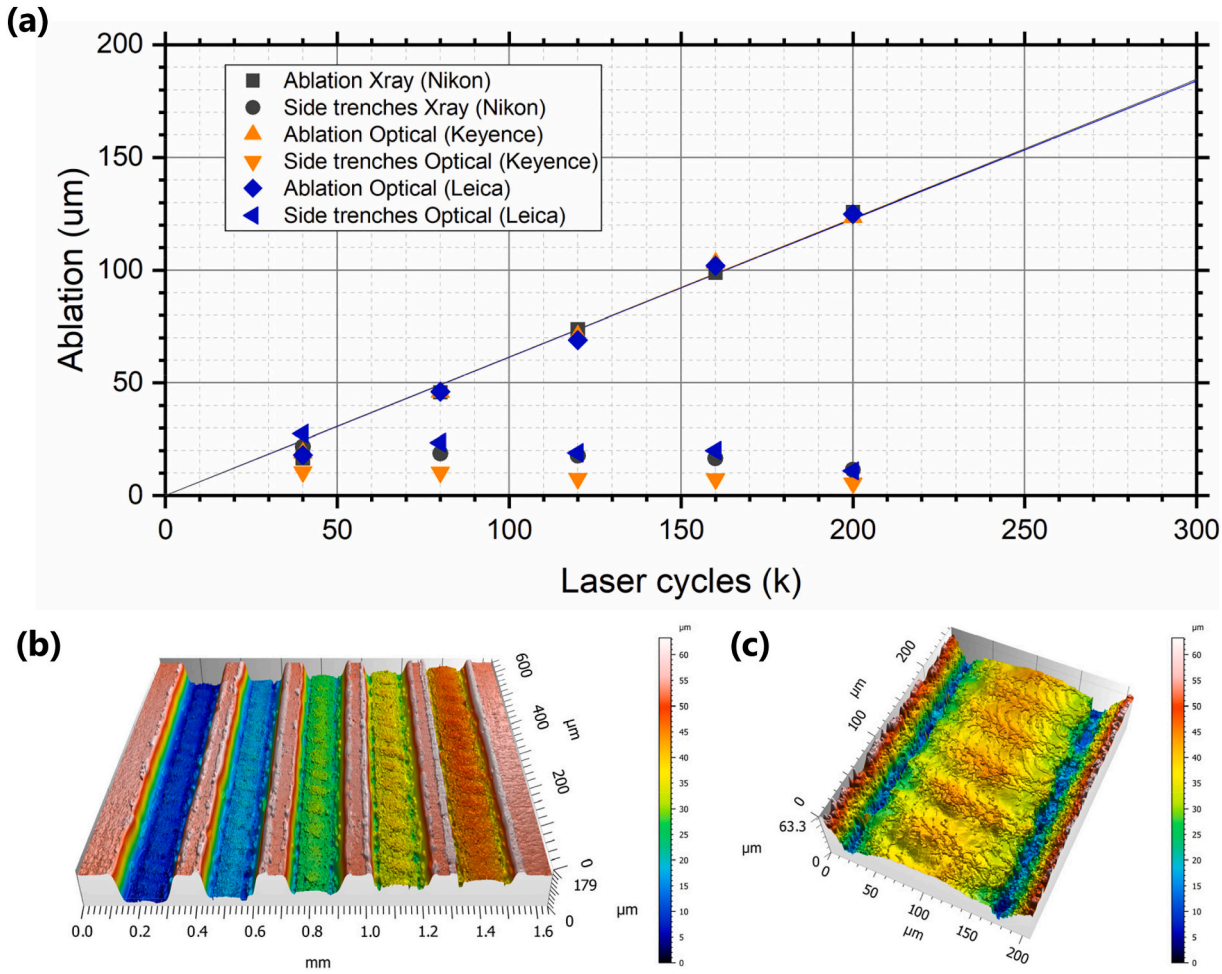

Fig. 4. Calibration lines showing the progression of laser cycles from 40,000 to 200,000. (a) Measurement of ablation depth and side trench depth using X-ray (Nikon), confocal microscope (Leica), and digital microscope (Keyence). (b) Graphic representation of the calibration trenches captured with Leica. (c) Zoomed-in view of the laser trench resulting from the application of 40,000 laser cycles (second trench from the right side of subimage (b)).

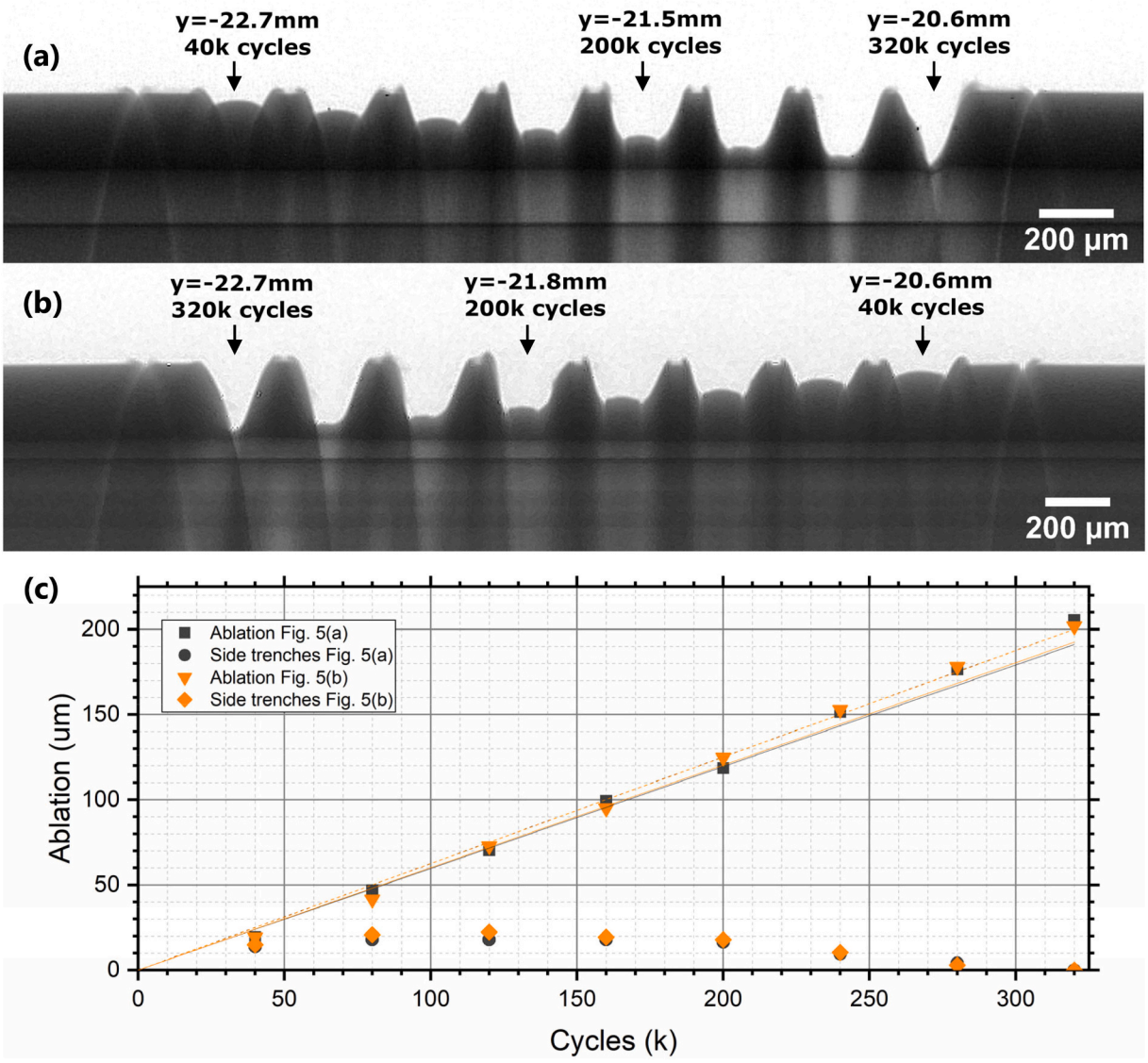

Fig. 5. X-ray images of calibration line series ranging from 40,000 to 320,000 laser cycles in increments of 40,000 laser cycles applied in close proximity to the bottom of the cell, in two different orders (a) and (b). (c) Ablation depth of the midline of the ablated line and the depth of the side trenches, using the data from panels a–b. The solid dark gray and orange lines represent the least squares linear interpolation with a constraint through the origin, using data points from 40,000 to 320,000 laser cycles. The dotted dark gray and orange lines represent the least squares linear interpolation through the origin, based on data points ranging from 40,000 to 200,000 laser cycles.

3.3. Limitation of laser ablation process

The redeposition of ablated steel material can lead to reduced width of the trench at higher ablation depths, as observed in Fig. 5(a–b). The method presented in this study successfully opens cells with wall thicknesses up to 240 µm from APR, Sony, Yinlong, and Samsung without any issues. However, if the wall thickness exceeds this limit, wider laser lines (>200 µm) and higher line spacing (>300 µm) are required. For validation purposes, calibration lines of up to 320,000 laser cycles are examined.

The proximity of the final laser trench to the cell's bottom side corresponds to a higher laser beam angle of incidence. As the trench gets deeper, it becomes narrower. This raises a question about how changing the order of laser cycles might affect the interpretation of calibration lines and the final laser trench depth. To address this, a y-coordinate is introduced parallel to the cell length. The y = 0.0 mm position represents the point below the laser lens, and y = −30.0 mm represents the end of the cell's bottom side. Calibration lines with a line spacing of 300 µm are placed near the cell's bottom side. This calibration lines span a range of 40,000 to 320,000 laser cycles in increments of 40,000 laser cycles.

In Fig. 5(a), the 40,000 laser cycle line is closer to the final laser trench and bottom of the cell than the 320,000 laser cycle line. Conversely, in Fig. 5(b), the 320,000 laser cycle line is closer to the final laser trench and bottom of the cell than the 40,000 laser cycle line.

The asymmetrical formation of the trench walls, visible between 200,000 and 320,000 laser cycles in Fig. 5(b), suggests an impact of the higher laser beam angle. To investigate this influence on the final laser trench depth, a least squares linear regression analysis is performed, with the intercept forced through zero. Considering the data up to 200,000 laser cycles, slopes of 5.972×10^{-4} µm/laser cycle (Fig. 5(a)) and 6.016×10^{-4} µm/laser cycle (Fig. 5(b)) are obtained.

The coefficient of determination (R^2), including the origin (0,0), excluding points >200,000 laser cycles, is 0.996 for Fig. 5(a) and 0.995 for Fig. 5(b).

As mentioned in Section 3.1, 300,000 laser cycles are required for the

desired ablation depth. The estimated ablation depth at 300,000 laser cycles is 188 μm for both methods (Fig. 5(a) and (b)). There is no relevant difference observed in calculating the laser depth between the two methods. However, due to the proximity of the final laser trench to the flat bottom side of the cell compared to the calibration series, it is advisable to use the method illustrated in Fig. 5(b).

Extending the analysis to 320,000 laser cycles, slopes of 6.253×10^{-4} μm/laser cycle (Fig. 5(a)) and 6.252×10^{-4} μm/laser cycle (Fig. 5 (b)) are obtained.

The coefficient of determination (R^2), including the origin (0,0) up to 320,000 laser cycles, is 0.998 for Fig. 5(a) and (b).

The estimated ablation depth at 300,000 laser cycles is 179 μm for Fig. 5(a) and 180 μm for Fig. 5(b). Taking into account the slight decrease in ablation depth per laser cycle at higher number of laser cycles, the estimated ablation depth is slightly lower when including data from 240,000 to 320,000 laser cycles. However, this difference, which is <10 μm, falls within the safety margin of 40 μm.

3.4. Number and position of the laser trenches

To facilitate the disconnection of electrode tabs and to minimize the risk of short circuits, it is recommended to apply laser trenches near the top and bottom sides. Insulating the cut tabs can provide additional protection against short circuits.

Ideally, the cell should be disassembled by opening the trenches at the top and bottom sides of the cell, as the middle section of the cell case is more susceptible to deformation than the areas near the top and bottom sides.

However, it is highly advised to include a calibration line series and incorporate a final laser trench in the middle of the cell case. This precautionary step helps in cases where the jelly roll adheres to the cell case, facilitating its removal.

To ensure an effective disassembly process, it is recommended to apply a total of three laser lines as shown in Fig. 1. By strategically placing these lines, the disassembly can be performed efficiently and with minimal risk of damage or complications.

3.5. Heat of laser applied to the cell

At temperatures above 80 °C, electrolyte decomposition may occur [58–60]. The initial decomposition of the solid electrolyte interface (SEI) takes place within the range of 80–130 °C [61,62]. Park et al. observed no decomposition of two SEI films on a graphite negative electrode until 60 °C [63], while Wang et al. demonstrated that SEI decomposition can start as low as 57 °C [64]. The optimal operating temperature range for lithium-ion batteries is 15–35 °C [65].

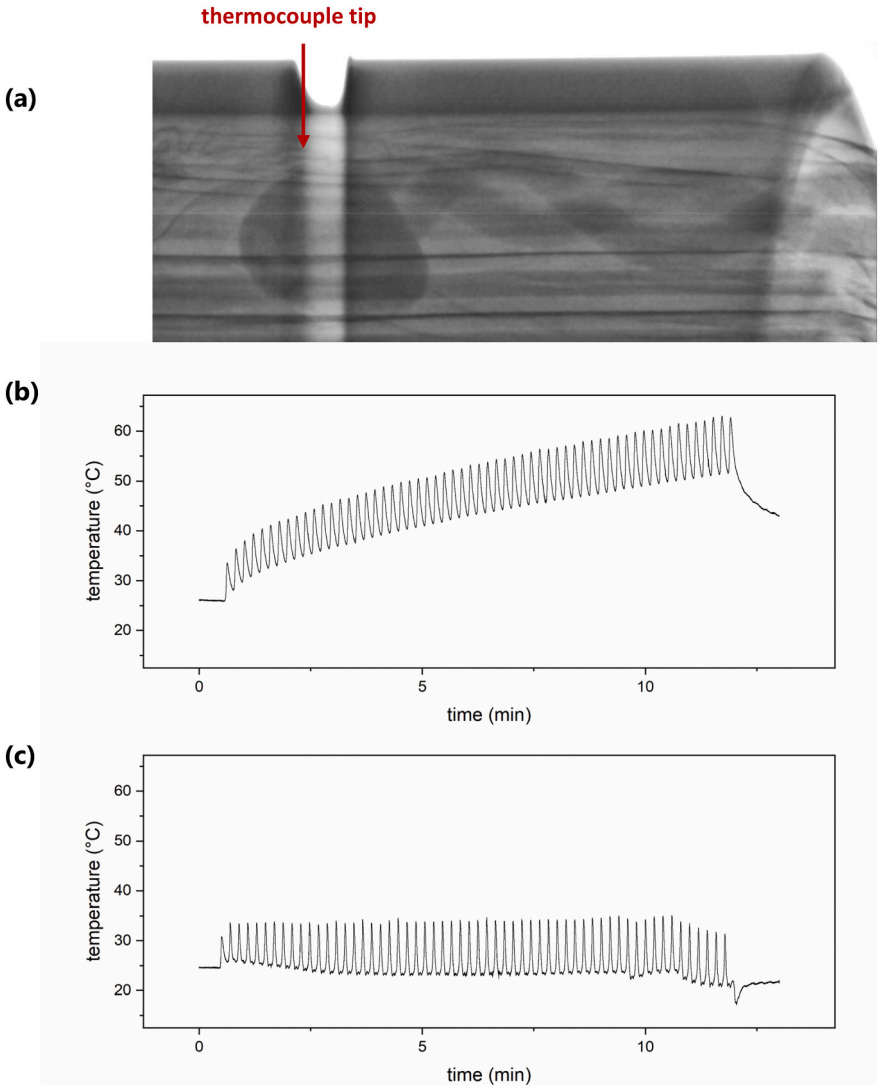

Fig. 6. In-situ temperature measurement. (a) X-ray image after 300,000 laser cycles without cooling, 6 W laser power. (b) temperature curve for 300,000 laser cycles without cooling, 6 W. (c) temperature curve for 300,000 laser cycles with active cooling, 6 W.

To avert potential harm to cell components, in-situ monitoring of temperature elevation was conducted using type K thermocouples (FLUKE 52 II Thermometer, CONDUSTRIE-MET AG, Wire diameter: 2 × 0.2 mm, spot-welded tip, Fig. 6(a), displays the thermocouple placement). The data was recorded at a sample rate of 100 Hz. The laser power was set to 6 W. This calibrated power parameter optimizes ablation time, reproducibility, and cell temperature increase. During the application of 300,000 laser cycles, the temperature within the cells increased from 26 °C to a maximal temperature of 63 °C. Fig. 6(b) depicts the temperature curve.

Localized temperature maxima arise solely when the laser aligns directly above the welded thermocouple tip, attributed to cell rotation. The temperature under the cell wall during laser treatment was mild due to the cell's rotation and the use of an optimized wobbling laser line. Overall, temperature values were notably lower than those reported in [58], confirming the thermal runaway safety of our approach. The laser heat input to the steel case is very localized, as [66] indicates. For post-mortem analysis, only portions at least 10 mm away from the final laser lines, were considered. Nonetheless, the authors aim to avoid the migration of decomposed material to the area of interest, requiring further process improvements.

The temperature increase under the cell case results from two factors: the overall increase of energy within the cell (baseline) and cyclic fluctuations (amplitude) per rotation cycle.

While a reduction in laser power from 6 W to 5 W decreased the cyclic amplitude from approximately 12 °C to 9 °C, it only partially addressed the issue of the overall temperature increase, see Fig. 6(b). The baseline increase remained high at +17 °C, in contrast to the original +26 °C without the reduction in laser power. In summary, the reduction in laser power increased the required cycle number by +65 % (496 k cycles), resulting in a temperature reduction of +12 °C.

A more efficient approach is to reduce the total heat accumulated in the cell by cooling it with pre-cooled air during laser ablation. Fig. 6(c) depicts the temperature change during 300,000 laser cycles. The amplitude per rotation in Fig. 6(c) is higher than in Fig. 6(b) due to the use of a new thermocouple with a smaller tip, providing higher time-resolution. In the last few laser cycles, as the wall thickness decreases and heat distribution in the cell case reduces, the amplitude increases. To maintain the maximum measured local temperature below 35 °C, the air stream was slightly increased in the last eleven laser cycles, causing a slight drop in the baseline in Fig. 6(c). After completing the laser ablation, the air stream valve was closed to avoid further cooling. According to Islava, radial cooling is preferred over axial cooling due to its larger surface area for heat transfer [67].

Pre-cooling of the cell was not required for this experiment, which would be an alternative way to reduce the maximum temperature. The entire equipment could also be stored within a climatized room, facilitating the thermal regulation of the cell during operation.

The experiment has clearly shown that actual temperature right on top of the jelly roll can be kept safe in terms of solid electrolyte interphase components' stability. By adjusting the air stream, the baseline of the temperature curve was kept more or less constant. The baseline is the temperature that is a good representation of the overall temperature of the cell close to the applied laser line. In practice, cooling with an air stream will be regulated to keep the outer cell case temperature constant. This is easily achieved by placing a thermocouple a few millimeters apart from one of the laser lines.

Online monitoring of the outer cell case during laser ablation operation with a thermocouple touching the cell case is a good indicator for keeping the cell temperature within a certain range. Frictional heat is negligibly small for the rotation speed at hand. This procedure will be more accurate than using a thermography camera for cells from other manufacturers where no thermocouple can be inserted.

3.6. Comparison of different disassembly techniques

Since the commencement of commercial production of cylindrical lithium-ion cells in 1991 by Sony Corporation, there has been a growing demand to disassemble these cells carefully for research purposes. Post-mortem analyses aiming at understanding failure and aging mechanisms and improving overall performance require meticulous disassembly [68,69].

The precision of the disassembly process significantly influences the outcomes of post-mortem analysis. Unfortunately, many researchers conducting these analyses have not been transparent about the disassembly methods employed within the glovebox.

As stated in the Introduction (Section 1), all currently reported techniques for disassembling cylindrical cells pose problems that need addressing. The main advantages and disadvantages of common techniques are summarized in Table 1.

Aurbach et al. were pioneers in conducting post-mortem analysis of lithium-ion batteries and proposed their approach for disassembling cylindrical cells in 2002 [70]. To ensure operator safety during disassembly, the entire disassembly process took place within a glovebox equipped with a remotely controlled X-Y moving stage. Their method involved an initial cut using a Dremel-based tool with a carbide-tipped saw, targeting the cap along the peripheral groove. Subsequently, they performed a longitudinal cut on the case to facilitate the easier removal of the jelly roll from the cell casing.

In 2011, Williard et al. [36] recommended a method for disassembling prismatic cells with a metal case, utilizing a Dremel tool to make a cut and employing pliers or wire cutters to pry back the top of the battery case. The top should still be connected on one side of the case to open it like a lid. At this point, the lid can be gripped with the pliers and twisted so that the battery casing begins to peel away from the internal jelly roll.

Williard et al. also emphasized the importance of caution when the cell is fixed in a vise or pliers are used during the removal of the safety circuit or the disassembly of the battery pack. Excessive compressive force can puncture the separator and short the anode and cathode. They also highlighted the risk of contamination due to the formed dust during cutting into the metal case.

Williard et al. cautioned against using pliers to peel off the cell case for cylindrical cells and instead suggested employing a Dremel-based saw tool, aligning with Aurbach et al.'s initial proposal. Notably, pictures from studies referenced in Table 1 revealed instances of mechanical destruction of samples when using the Dremel tool.

In 2016, Waldmann et al. proposed using a Dremel for top cap removal after an interior cell examination, recommending non-destructive characterization techniques such as X-ray analysis from various angles or X-ray computed tomography (CT), which aligns with our methodology. They expressed concerns about the potential generation of local heat during cutting and the formation of lengthy swarfs that could lead to short circuits. They emphasized the need for the cell opening process to be carried out meticulously, with avoidance of excessive force on the jelly roll. Additionally, they issued a warning about the risk of external short circuits due to unintentional contact with external tabs, conductive tools, metal flakes during cutting, or contact with the metallic surface of the glovebox [26].

Somerville's extensive work in 2017, analyzing electrode samples with a Dremel tool, revealed speckles on electrodes containing carbon, oxygen, and trace amounts of metals such as copper, manganese, and iron [57]. When Somerville disassembled the cells using a pipe cutter and pliers, he did not examine these speckles. He employed the pipe cutter for top cap removal and pliers for peeling off the cell case. He concluded that the use of a Dremel tool disperses dust, particles, and other materials throughout the environment during the cutting and electrode removal process, which is unfavorable when unwinding the jelly roll within the same glovebox. Instead of this method, he advised using a pipe cutter. He writes: "This new method does not create dust,

Table 1
Comparison of different disassembly methods for cylindrical battery cells (the higher placed in the table, the higher the estimated practical relevance).

Method	References	Benefits	Drawbacks	Equipment cost	Time
X-ray, laser ablation, with water pump plier	[N/A]	• Safe method; suitable for disassembling cells at different states of charges	• Build-up of initial experience required	Medium	Low for known cell (see below)
Pipe cutter with (sharp needle-nose) plier	[52–54,80–88]	• No swarfs • Low risk of short-circuits by removing the positive terminal	• Risk of short-circuits • Risk of mechanical deformation during peeling off the case with pliers	Low	Low
Sawing high precision saw; CNC mill machine	[83–86,51,55,70,89–91]	• Accurate removal of steel if circularity of cylindrical cell is given (was often not the case in the cells we have tested) • Useful for disassembling prismatic cells	• Usually cell is not circular enough, leading to different removal depth • Space requirement of a CNC (alternatives) • Accuracy: 50 µm of a small precision saw as the disassembly lathe MTI MSK-530	Medium -high	Medium
Sawing dremel with carbide-tipped saw	[2,36,57,70,80,92–98]	• Cheap and fast	• Risk of short-circuits • Metal dust and swarfs (SEI altered) • Carbide-tipped saw: black soot might taint the electrodes • Local temperature increase • Short lifetime of brush motors in argon atmosphere (avoidable)	Low	Low
Pipe applied on both cell peripheries	[99,100]	• Cheap and fast	• Risk of short-circuits due to mechanical deformation of the jelly roll • Not as reproducible as our proposed laser ablation method	Low	Low
Piercing awl with (sharp needle-nose) plier	[N/A]	• Piercing a small hole at the bottom center in the mandrel hole and peeling off the case seems risky	• Risk of short-circuits • Risk of mechanical deformation of the jelly roll	Low	Low
Manual (sharp needle-nose or diagonal) plier, ceramic knife, scalpel, scissor	[17,101–103]	• Cheap and fast • Scissors/scalpels only recommended for pouch cells	• Risk of short-circuits by damaging the sealing gasket • Risk of damaging personal equipment/gloves • Risk of mechanical deformation of the jelly roll	Low	Medium

particles, or metal shards. It avoids cutting into the electrode materials, uses fewer resources, is less convoluted, and can be performed in a similar period of time. No contaminants were found in cells that were opened using this method, and therefore, it should be adopted."

Concerns about metal dust release during sawing led us to discourage the carbide-tipped saw tool proposed by Aurbach et al. in 2002.

To mitigate the particles resulting from laser ablation of the cell cases, we clean our cell cases with ethanol post-ablation. This process removes all metal nanoparticles and dust. Additionally, we eliminate any leftover solvents using compressed air and place the cells in the glovebox antechamber under vacuum.

Spielbauer et al. investigated the impact of mechanical deformation on the aging, safety, and electrical behavior of 18650 lithium-ion battery cells, observing imprints of the current collector on electrodes [71,72]. Mechanical stress is a critical factor to address and analyze, especially for new cell chemistries [73,74]. Even current Li-ion cells can experience jelly roll deformation [75]. Consequently, we believe that peeling off the steel case with pliers might exacerbate electrode deformation in worst-case scenarios. With our method, we can disassemble cylindrical cells that have already undergone electrode fracture [76].

Initially, we utilized our marking laser to remove the cell case on both peripheries of a fully discharged cell. Subsequently, within the fume hood, we effortlessly extracted the jelly roll. As detailed in Section 2.3, we recognized that breaking the residual wall thickness of 40 µm and removing the jelly roll from the cell case demands only minimal mechanical force, underscoring the efficacy of our approach.

While acknowledging that using a pipe cutter to remove the top cap, followed by pliers to detach the case, was likely the safest approach before our methodology, we are concerned that using pliers to peel off the case may cause mechanical damage to the jelly roll.

We looked for alternative ways to remove the jelly roll without the need of peeling off the case with pliers and tested pipe cutters and an axle turning lathe.

Pipe cutters provide a fast and cost-effective approach for disassembling cylindrical cells. However, using a pipe cutter from both sides of the cell (near the top and bottom) can result in significant non-uniformity in the depth of steel removal, as shown in Fig. 7. This figure was made by applying 25 turns within a pipe cutter (TUBE CUTTER 35, 6-35 mm, DURAMAG). We have evaluated different types of tube cutters; all of them seem to mechanically deform the jelly roll. Furthermore, the use of pipe cutters, risk electrical short circuits. According to Somerville (2017), the method they used was safe, only one of 63 cells used was has experienced a short-circuit [57]. Their method included peeling of the can with pliers.

A safer approach is to prepare a breaking line outside the glovebox and breach the ablated wall within the glovebox. For this purpose, a turning lathe or CNC lathe could be utilized. However, it is important to consider that the ablation achieved with a CNC mill may not always be uniform due to steel wall deformation and variations in wall thickness. One battery cell was prepared with an axle turning lathe. The cell outer diameter, was measured with an electrical caliper (Toolcraft TO-5664642), was found to be 17.81 mm and 17.85 mm at different rotational orientations, indicating that the cell is not perfectly round. The result is shown in Fig. 8. CNC lathe require space and are expensive. CNC machines have potential for material recovery of cylindrical cells [55].

Initially, we considered acquiring a small, high-precision saw that could be installed within our glovebox or a specifically designed tool for disassembling 18650-type battery cells, such as the MTI product (MSK-

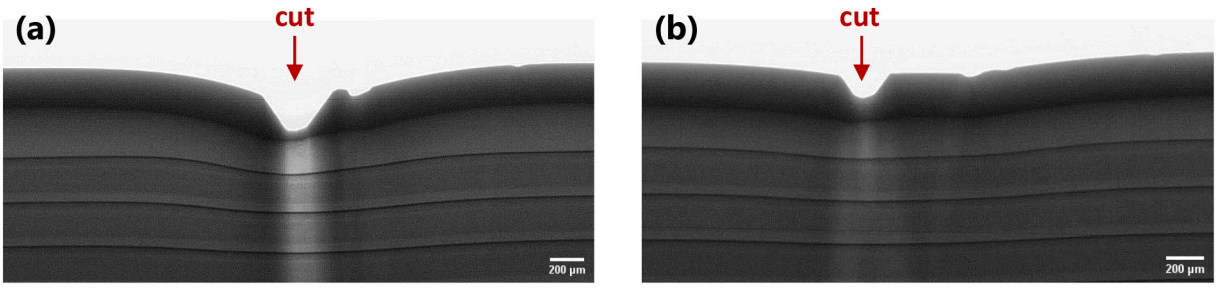

Fig. 7. X-ray image of a cylindrical cell processed with a pipe cutter, consisting of 25 turns. Both subimages (a) and (b) show the same cut, at two different rotational orientations.

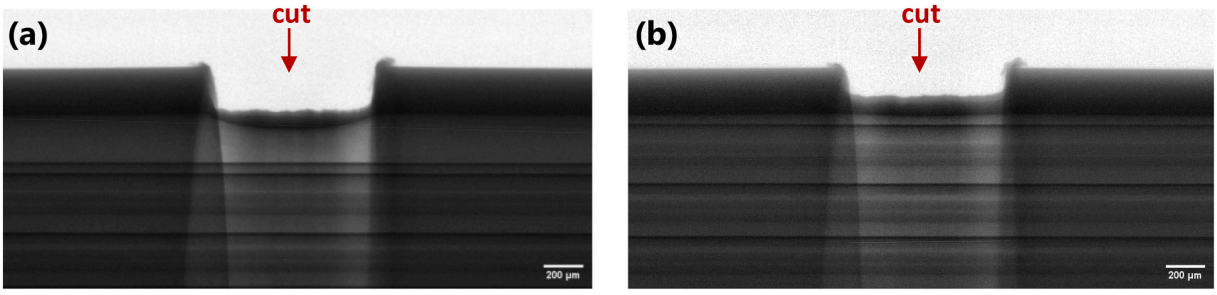

Fig. 8. X-ray image of a cylindrical cell processed with a turning lathe. Both subimages (a) and (b) show the same cut, at two different rotational orientations.

530). However, these low-budget tools typically offer an accuracy ranging between 20 and 50 µm, making them unsuitable for our needs, especially for the protective insulating material around the jelly roll, which has a thickness of a few micrometers. We contemplated applying a cut with a safety margin outside our glovebox using a high-precision axle lathe and breaking the safety margin within the glovebox with water pump pliers.

Pre-tests with a pipe cutter and an axle lathe revealed that both tools are inappropriate for non-perfectly circular cells, as was the case for our samples. Concerns arose about potential damage if a cell underwent a breach in the case under air or if the cut occurred within the electrode materials. Having previously established the laser ablation variation to be within 5–10 µm, we explored various safety margins.

To ensure the safety and reliability of our process, we immersed over ten fully discharged cells in a water bath with a safety margin of <10 µm, applying a vacuum above the vapor pressure of water. Cells with even a minor breach, not visible to the naked eye, exhibited strong bubbling at the holes, attributed to the evaporation of low-volatile electrolyte components. Furthermore, we observed that the cell wall safety margin of 40 µm was robust enough to withstand a vacuum of 0.1 mbar abs. (-1 bar rel.). While the majority of cells remained tight above 20 µm, we increased the safety margin to 40 µm, maintaining safety for a potential presence of slight gas pressure within the cell.

For applying three cuts with a safety margin and breaking the rest of the wall within the glovebox with water pump pliers, we believe neither the CNC nor the Dremel is appropriate due to the uncertainty caused by the non-circular behavior of many cylindrical cells. This process would have to be carried out within an inert atmosphere, such as an argon-purged glovebox. We also believe that both mechanical tools might generate enough heat to alter the SEI components, and cooling within the glovebox would not be a straightforward solution.

Our method works well even if the cylindrical cell has slight non-circularity. Abnormal high non-circularity would be observed during the calibration series within the X-ray machine when some parts of the cell show less ablation than others.

Some of the jelly rolls are wrapped with additional protective insulating foils, and some are not. Some cylindrical cells come with protective devices, while others lack them. The effectiveness of specific state-of-the-art disassembly methods, such as working with pliers or a Dremel-like saw tool, may depend on the specific components used during cell assembly [77]. Our method works with every cylindrical cell of the type 18650, without the need for pretests with other cells, making it the ultimate solution for a safe post-mortem analysis.

In the reviewed research articles, the cells were typically discharged to their respective end-of-discharge voltage. For example, Waldmann et al. discharged cells to an end-of-discharge voltage of 2.0 V, to minimize both risk and corrosion issues [51]. The main advantage of the laser method is, that a cell does not need to be fully discharged prior post-operational analysis, since the laser ablation assisted disassembly method does not pose any risk. This allows the analysis of elemental distribution at State of Charge (SoC).

For the execution of X-ray measurements, calibration series, determining the required laser cycle number, and applying final laser lines on a single cell, approximately one person-hour is needed, showcasing the efficiency. Following the assessment of three cells from the same production lot, each having identical wall thickness and ablation properties, the preparation of laser lines for disassembly in the glovebox required an additional quarter hour for each cell. An X-ray machine serves as an invaluable addition for in-depth post-mortem analysis [30].

Braking the laser lines within the glovebox was achieved by us within 1 min, which is important when there is a need to recover as much highly volatile electrolyte as possible for electrolyte composition analysis [78]. Applying 300,000 laser cycles for the tested cell with a wall thickness of 231 µm consumed less than a quarter hour. Depending on the cell manufacturing, we believe it is reasonable to disassemble one cylindrical cell with known parameters (ablation speed and wall thickness) with one final laser line within <20 min, which will be interesting when analyzing lithium plating. This process should be analyzed after the occurring event as soon as possible [61,79].

Overall, the proposed 2D-X-ray assisted laser ablation method with cracking the final laser lines with water pump pliers within the glovebox, avoids all the mentioned issues and guarantees a safe, reproducible and efficient method for disassembling cylindrical cells.

4. Conclusion

This study introduces a novel laser ablation assisted disassembly process with X-ray and optical validation for cylindrical battery cells, specifically the commonly used 18650 type. The method preserves the jelly roll, making it suitable for failure analysis and degradation research of the cell's active materials, benefiting cell producers, testing laboratories, and research institutes. The process is not limited to the investigated cells and can be applied to various cylindrical battery cell formats, expanding its applicability.

The redeposition of ablated material and side trench formation has been effectively addressed. Cells from various manufacturers, with wall thickness up to 240 μm, were opened using the presented procedure. For thicker walls, wider laser lines and higher line spacing are necessary.

The cell opening process is demonstrated to be safe and reproducible, achieving a laser trench depth of 188 ± 4 μm (1 SD, 8 cells) for cells with a wall thickness of 231 ± 1 μm (1 SD, 8 cells). A safety margin of 10 to 20 μm is necessary to accommodate non-uniform cell housings, while a margin of 40 μm ensures both sufficient breakability of the cell wall and mechanical stability.

In-situ temperature measurements confirm a moderate temperature increase beneath the cell case. Notably, a peak temperature of 62 °C was observed during the laser ablation process, which is well below the safety-critical thermal-runaway threshold of 80 °C. To ensure that the inner cell temperature remains below the reported SEI-decomposition onset temperature of 57 °C, it is crucial to cool the cylindrical cell during operation. By cooling down the cell with pre-cooled air, the temperature during laser operation was maintained in the range of 17 °C and 35 °C.

In conclusion, this comprehensive and innovative approach provides reliable and efficient disassembly of cylindrical battery cells. The combination of X-ray and optical validation enables precise measurement and evaluation of wall thickness and trench depth, facilitating detailed failure analysis and investigation of aging effects. These findings contribute to the advancement of battery research and manufacturing.

In conclusion, we are confident that our methodology is not only effective but also proves to be efficient in terms of overall costs.

Further research is recommended to evaluate the applicability and effectiveness of the proposed method on prismatic cells with metal housing and coin cells. Proper drying or washing procedures should be implemented when analyzing the anode and cathode active materials to avoid moisture traces. These extensions will provide valuable insights into material analysis in batteries across different cell types.

Declaration of artificial intelligence (AI) and AI-assisted technologies in the writing process

Statement: During the preparation of this work the author(s) used ChatGPT (OpenAI) to improve readability and language. Following the use of these tools/services, the author(s) carefully reviewed and edited the content as necessary. The author(s) take(s) full responsibility for the accuracy and content of the publication.

CRediT authorship contribution statement

Daniel Aeppli: Conceptualization, Formal analysis, Investigation, Methodology, Validation, Visualization, Writing – original draft, Writing – review & editing. **Jonas Gartmann:** Methodology. **René Schneider:** Investigation, Visualization. **Erwin Hack:** Formal analysis, Writing – review & editing. **Sebastian Kretschmer:** Conceptualization. **Thi Thu Dieu Nguyen:** Conceptualization. **Marcel Held:** Conceptualization, Project administration, Supervision, Writing – review & editing.

Declaration of competing interest

The authors declare that they have no known competing financial interests or personal relationships that could have appeared to influence the work reported in this paper.

Data availability

Data will be made available on request.

Acknowledgments

DN is grateful for financial support of ETH foundation and Swiss Federal Office of Energy as part of the ReMap project. We are also grateful to Robin Bucher, Erwin Pieper and his team from Empa for their contribution.

References

[1] G. Berdichevsky, K. Kelty, J. Straubel, E. Toomre, The Tesla Roadster Battery System Tesla Motors, Inc. 04, 2006.
[2] S. Baazouzi, N. Feistel, J. Wanner, I. Landwehr, A. Fill, K.P. Birke, Design, properties, and manufacturing of cylindrical Li-ion battery cells—a generic overview, Batteries 9 (2023) 309, https://doi.org/10.3390/batteries9060309.
[3] C. Pillot, The Rechargeable Battery Market and Main Trends 2020–2030. https://www.crepim.fr/DOCS_CLIENT/Batteries%20Market%20in%202020%20by%20technology,%20applications%20&%20battery%20suppliers-Li-ion%20components%20market%20&%20value%20chain-Raw%20materials%20market%20Supplier-Raw%20material%20cost-Ne.pdf, 2021. (Accessed 4 July 2023).
[4] Global Cylindrical Lithium-Ion Battery Market Report and Forecast 2023-2028, (n.d.). https://www.expertmarketresearch.com/reports/cylindrical-lithium-ion-battery-market (accessed June 28, 2023).
[5] M.D.F. ltd, Cylindrical Lithium Battery Pack Market | Size | 2023 to 2028, Market Data Forecast. (n.d.). https://www.marketdataforecast.com/market-reports/cylindrical-lithium-battery-pack-market (accessed June 26, 2023).
[6] J.M. Granholm, National Blueprint for Lithium Batteries 2021–2030, (n.d.). https://www.energy.gov/sites/default/files/2021-06/FCAB%20National%20Blueprint%20Lithium%20Batteries%200621_0.pdf (accessed July 4, 2023).
[7] P.H. Camargos, P.H.J. dos Santos, I.R. dos Santos, G.S. Ribeiro, R.E. Caetano, Perspectives on Li-ion battery categories for electric vehicle applications: a review of state of the art, Int. J. Energy Res. 46 (2022) 19258–19268, https://doi.org/10.1002/er.7993.
[8] M. Li, J. Lu, Z. Chen, K. Amine, 30 years of lithium-ion batteries, Adv. Mater. 30 (2018) 1800561, https://doi.org/10.1002/adma.201800561.
[9] X.-Y. Yao, M.G. Pecht, Tab Design and failures in cylindrical Li-ion batteries, IEEE Access 7 (2019) 24082–24095, https://doi.org/10.1109/ACCESS.2019.2899793.
[10] BU-301a: Types of Battery Cells, Battery University, 2010. https://batteryuniversity.com/article/bu-301a-types-of-battery-cells. (Accessed 28 June 2023).
[11] L. Wang, S. Yin, Z. Yu, Y. Wang, T.X. Yu, J. Zhao, Z. Xie, Y. Li, J. Xu, Unlocking the significant role of shell material for lithium-ion battery safety, Mater. Des. 160 (2018) 601–610, https://doi.org/10.1016/j.matdes.2018.10.002.
[12] L.N. Trinh, D. Lee, The characteristics of laser welding of a thin aluminum tab and steel battery case for lithium-ion battery, Metals 10 (2020) 842, https://doi.org/10.3390/met10060842.
[13] S. Malmgren, Insights Into Li-ion Battery and Stainless Steel Interfaces Using Refined Photoelectron Spectroscopy Methodology. https://urn.kb.se/resolve?urn=urn:nbn:se:uu:diva-197153, 2013. (Accessed 5 July 2023).
[14] M. Shahjalal, P.K. Roy, T. Shams, A. Fly, J.I. Chowdhury, Md.R. Ahmed, K. Liu, A review on second-life of Li-ion batteries: prospects, challenges, and issues, Energy 241 (2022) 122881, https://doi.org/10.1016/j.energy.2021.122881.
[15] J. Schäfer, R. Singer, J. Hofmann, J. Fleischer, Challenges and solutions of automated disassembly and condition-based remanufacturing of lithium-ion battery modules for a circular economy, Procedia Manuf. 43 (2020) 614–619, https://doi.org/10.1016/j.promfg.2020.02.145.
[16] M. Pagliaro, F. Meneguzzo, Lithium battery reusing and recycling: a circular economy insight, Heliyon 5 (2019) e01866, https://doi.org/10.1016/j.heliyon.2019.e01866.
[17] J. Marshall, D. Gastol, R. Sommerville, B. Middleton, V. Goodship, E. Kendrick, Disassembly of Li ion cells—characterization and safety considerations of a recycling scheme, Metals 10 (2020) 773, https://doi.org/10.3390/met10060773.
[18] M.H.S.M. Haram, J.W. Lee, G. Ramasamy, E.E. Ngu, S.P. Thiagarajah, Y.H. Lee, Feasibility of utilising second life EV batteries: applications, lifespan, economics, environmental impact, assessment, and challenges, Alex. Eng. J. 60 (2021) 4517–4536, https://doi.org/10.1016/j.aej.2021.03.021.
[19] H. Ali, H.A. Khan, M. Pecht, Preprocessing of spent lithium-ion batteries for recycling: need, methods, and trends, Renew. Sust. Energ. Rev. 168 (2022) 112809, https://doi.org/10.1016/j.rser.2022.112809.
[20] G. Harper, R. Sommerville, E. Kendrick, L. Driscoll, P. Slater, R. Stolkin, A. Walton, P. Christensen, O. Heidrich, S. Lambert, A. Abbott, K. Ryder, L. Gaines, P. Anderson, Recycling lithium-ion batteries from electric vehicles, Nature 575 (2019) 75–86, https://doi.org/10.1038/s41586-019-1682-5.
[21] O. Groux, In-house Recycling von Li-Ionenbatterien: Alternativen zu etablierten Recyclingoptionen unter Beachtung rechtlicher und sicherheitstechnischer Auflagen, bachelorthesis, 2018.

[22] S. Doose, J.K. Mayer, P. Michalowski, A. Kwade, Challenges in ecofriendly battery recycling and closed material cycles: a perspective on future lithium battery generations, Metals 11 (2021) 291, https://doi.org/10.3390/met11020291.
[23] G.D.J. Harper, E. Kendrick, P.A. Anderson, W. Mrozik, P. Christensen, S. Lambert, D. Greenwood, P.K. Das, M. Ahmeid, Z. Milojevic, W. Du, D.J.L. Brett, P. R. Shearing, A. Rastegarpanah, R. Stolkin, R. Sommerville, A. Zorin, J.L. Durham, A.P. Abbott, D. Thompson, N.D. Browning, B.L. Mehdi, M. Bahri, F. Schanider-Tontini, D. Nicholls, C. Stallmeister, B. Friedrich, M. Sommerfeld, L.L. Driscoll, A. Jarvis, E.C. Giles, P.R. Slater, V. Echavarri-Bravo, G. Maddalena, L.E. Horsfall, L. Gaines, Q. Dai, S.J. Jethwa, A.L. Lipson, G.A. Leeke, T. Cowell, J.G. Farthing, G. Mariani, A. Smith, Z. Iqbal, R. Golmohammadzadeh, L. Sweeney, V. Goodship, Z. Li, J. Edge, L. Lander, V.T. Nguyen, R.J.R. Elliot, O. Heidrich, M. Slattery, D. Reed, J. Ahuja, A. Cavoski, R. Lee, E. Driscoll, J. Baker, P. Littlewood, I. Styles, S. Mahanty, F. Boons, Roadmap for a sustainable circular economy in lithium-ion and future battery technologies, J. Phys. Energy 5 (2023) 021501, https://doi.org/10.1088/2515-7655/acaa57.
[24] A. Friesen, X. Mönnighoff, M. Börner, J. Haetge, F.M. Schappacher, M. Winter, Influence of temperature on the aging behavior of 18650-type lithium ion cells: a comprehensive approach combining electrochemical characterization and post-mortem analysis, J. Power Sources 342 (2017) 88–97, https://doi.org/10.1016/j.jpowsour.2016.12.040.
[25] A. Friesen, F. Horsthemke, X. Mönnighoff, G. Brunklaus, R. Krafft, M. Börner, T. Risthaus, M. Winter, F.M. Schappacher, Impact of cycling at low temperatures on the safety behavior of 18650-type lithium ion cells: combined study of mechanical and thermal abuse testing accompanied by post-mortem analysis, J. Power Sources 334 (2016) 1–11, https://doi.org/10.1016/j.jpowsour.2016.09.120.
[26] T. Waldmann, A. Iturrondobeitia, M. Kasper, N. Ghanbari, F. Aguesse, E. Bekaert, L. Daniel, S. Genies, I.J. Gordon, M.W. Löble, E.D. Vito, M. Wohlfahrt-Mehrens, Review—post-mortem analysis of aged lithium-ion batteries: disassembly methodology and physico-chemical analysis techniques, J. Electrochem. Soc. 163 (2016) A2149, https://doi.org/10.1149/2.1211609jes.
[27] C.R. Birkl, M.R. Roberts, E. McTurk, P.G. Bruce, D.A. Howey, Degradation diagnostics for lithium ion cells, J. Power Sources 341 (2017) 373–386, https://doi.org/10.1016/j.jpowsour.2016.12.011.
[28] T. Waldmann, S. Gorse, T. Samtleben, G. Schneider, V. Knoblauch, M. Wohlfahrt-Mehrens, A mechanical aging mechanism in lithium-ion batteries, J. Electrochem. Soc. 161 (2014) A1742–A1747, https://doi.org/10.1149/2.1001410jes.
[29] B. Gyenes, D.A. Stevens, V.L. Chevrier, J.R. Dahn, Understanding anomalous behavior in coulombic efficiency measurements on Li-ion batteries, J. Electrochem. Soc. 162 (2014) A278, https://doi.org/10.1149/2.0191503jes.
[30] A. Pfrang, A. Kersys, A. Kriston, D.U. Sauer, C. Rahe, S. Käbitz, E. Figgemeier, Long-term cycling induced jelly roll deformation in commercial 18650 cells, J. Power Sources 392 (2018) 168–175, https://doi.org/10.1016/j.jpowsour.2018.03.065.
[31] H. Wang, J.F. Whitacre, Inhomogeneous aging of cathode materials in commercial 18650 lithium ion battery cells, J. Energy Storage 35 (2021) 102244, https://doi.org/10.1016/j.est.2021.102244.
[32] M. Uitz, M. Sternad, S. Breuer, C. Täubert, T. Traußnig, V. Hennige, I. Hanzu, M. Wilkening, Aging of tesla's 18650 lithium-ion cells: correlating solid-electrolyte-interphase evolution with fading in capacity and power, J. Electrochem. Soc. 164 (2017) A3503–A3510, https://doi.org/10.1149/2.0171714jes.
[33] M. Börner, A. Friesen, M. Grützke, Y.P. Stenzel, G. Brunklaus, J. Haetge, S. Nowak, F.M. Schappacher, M. Winter, Correlation of aging and thermal stability of commercial 18650-type lithium ion batteries, J. Power Sources 342 (2017) 382–392, https://doi.org/10.1016/j.jpowsour.2016.12.041.
[34] H. Sharifi, B. Mosallanejad, M. Mohammadzad, S.M. Hosseini-Hosseinabad, S. Ramakrishna, Cycling performance of LiFePO4/graphite batteries and their degradation mechanism analysis via electrochemical and microscopic techniques, Ionics 28 (2022) 213–228, https://doi.org/10.1007/s11581-021-04258-9.
[35] C. Hendricks, N. Williard, S. Mathew, M. Pecht, A failure modes, mechanisms, and effects analysis (FMMEA) of lithium-ion batteries, J. Power Sources 297 (2015) 113–120, https://doi.org/10.1016/j.jpowsour.2015.07.100.
[36] N. Williard, B. Sood, M. Osterman, M. Pecht, Disassembly methodology for conducting failure analysis on lithium–ion batteries, J. Mater. Sci. Mater. Electron. 22 (2011) 1616–1630, https://doi.org/10.1007/s10854-011-0452-4.
[37] J. Liu, Q. Duan, W. Peng, L. Feng, M. Ma, S. Hu, J. Sun, Q. Wang, Slight overcharging cycling failure of commercial lithium-ion battery induced by the jelly roll destruction, Process Saf. Environ. Prot. 160 (2022) 695–703, https://doi.org/10.1016/j.psep.2022.02.067.
[38] J.S. Edge, S. O'Kane, R. Prosser, N.D. Kirkaldy, A.N. Patel, A. Hales, A. Ghosh, W. Ai, J. Chen, J. Yang, S. Li, M.-C. Pang, L.B. Diaz, A. Tomaszewska, M. W. Marzook, K.N. Radhakrishnan, H. Wang, Y. Patel, B. Wu, G.J. Offer, Lithium ion battery degradation: what you need to know, Phys. Chem. Chem. Phys. 23 (2021) 8200–8221, https://doi.org/10.1039/D1CP00359C.
[39] R. Stockhausen, L. Gehrlein, M. Müller, T. Bergfeldt, A. Hofmann, F.J. Müller, J. Maibach, H. Ehrenberg, A. Smith, Investigating the dominant decomposition mechanisms in lithium-ion battery cells responsible for capacity loss in different stages of electrochemical aging, J. Power Sources 543 (2022) 231842, https://doi.org/10.1016/j.jpowsour.2022.231842.
[40] G. Bouteau, A.N. Van-Nhien, M. Sliwa, N. Sergent, J.-C. Lepretre, G. Gachot, I. Sagaidak, F. Sauvage, Effect of standard light illumination on electrolyte's stability of lithium-ion batteries based on ethylene and di-methyl carbonates, Sci. Rep. 9 (2019) 135, https://doi.org/10.1038/s41598-018-36836-9.
[41] S.J. An, J. Li, C. Daniel, D.L. Wood, Effects of ultraviolet light treatment in ambient air on lithium-ion battery graphite and PVDF binder, J. Electrochem. Soc. 166 (2019) A1121, https://doi.org/10.1149/2.0591906jes.
[42] S.J. An, J. Li, Y. Sheng, C. Daniel, D.L. Wood, Long-term lithium-ion battery performance improvement via ultraviolet light treatment of the graphite anode, J. Electrochem. Soc. 163 (2016) A2866, https://doi.org/10.1149/2.0171614jes.
[43] R. Omrani, Experimental Study and Modeling for the Safety of Li-ion Batteries, phdthesis, 2022.
[44] M. Kosfeld, B. Westphal, A. Kwade, Moisture behavior of lithium-ion battery components along the production process, J. Energy Storage 57 (2023) 106174, https://doi.org/10.1016/j.est.2022.106174.
[45] J.K. Mayer, F. Huttner, C.A. Heck, D. Steckermeier, M.-W. von Horstig, A. Kwade, Investigation of moisture content, structural and electrochemical properties of nickel-rich NCM based cathodes processed at ambient atmosphere, J. Electrochem. Soc. 169 (2022) 060512, https://doi.org/10.1149/1945-7111/ac7358.
[46] F. Orsini, A. Du Pasquier, B. Beaudoin, J.M. Tarascon, M. Trentin, N. Langenhuizen, E. De Beer, P. Notten, In situ Scanning Electron Microscopy (SEM) observation of interfaces within plastic lithium batteries, J. Power Sources 76 (1998) 19–29, https://doi.org/10.1016/S0378-7753(98)00128-1.
[47] S.J. An, J. Li, C. Daniel, D. Mohanty, S. Nagpure, D.L. Wood, The state of understanding of the lithium-ion-battery graphite solid electrolyte interphase (SEI) and its relationship to formation cycling, Carbon 105 (2016) 52–76, https://doi.org/10.1016/j.carbon.2016.04.008.
[48] P. Verma, P. Maire, P. Novák, A review of the features and analyses of the solid electrolyte interphase in Li-ion batteries, Electrochim. Acta 55 (2010) 6332–6341, https://doi.org/10.1016/j.electacta.2010.05.072.
[49] C. Mikolajczak, M. Kahn, K. White, R.T. Long, Lithium-ion Batteries Hazard and Use Assessment, Springer US, Boston, MA, 2011, https://doi.org/10.1007/978-1-4614-3486-3.
[50] D.L. Thompson, J.M. Hartley, S.M. Lambert, M. Shiref, G.D.J. Harper, E. Kendrick, P. Anderson, K.S. Ryder, L. Gaines, A.P. Abbott, The importance of design in lithium ion battery recycling – a critical review, Green Chem. 22 (2020) 7585–7603, https://doi.org/10.1039/D0GC02745F.
[51] T. Waldmann, M. Wilka, M. Kasper, M. Fleischhammer, M. Wohlfahrt-Mehrens, Temperature dependent ageing mechanisms in Lithium-ion batteries – a post-mortem study, J. Power Sources 262 (2014) 129–135, https://doi.org/10.1016/j.jpowsour.2014.03.112.
[52] Y. Yu, T. Vincent, J. Sansom, D. Greenwood, J. Marco, Distributed internal thermal monitoring of lithium ion batteries with fibre sensors, J. Energy Storage 50 (2022) 104291, https://doi.org/10.1016/j.est.2022.104291.
[53] A. Ghannoum, R.C. Norris, K. Iyer, L. Zdravkova, A. Yu, P. Nieva, Optical characterization of commercial lithiated graphite battery electrodes and in situ fiber optic evanescent wave spectroscopy, ACS Appl. Mater. Interfaces 8 (2016) 18763–18769, https://doi.org/10.1021/acsami.6b03638.
[54] R. Norris, K. Iyer, V. Chabot, P. Nieva, A. Yu, A. Khajepour, J. Wang, Multi-band reflectance spectroscopy of carbonaceous lithium iron phosphate battery electrodes versus state of charge, in: Optical Components and Materials XI, SPIE, 2014, pp. 260–267, https://doi.org/10.1117/12.2040655.
[55] H. Bi, H. Zhu, L. Zu, Y. Gao, S. Gao, Y. Bai, Environment-friendly technology for recovering cathode materials from spent lithium iron phosphate batteries, Waste Manag. Res. 38 (2020) 911–920, https://doi.org/10.1177/0734242X20931933.
[56] Y. Lu, M. Maftouni, T. Yang, P. Zheng, D. Young, Z.J. Kong, Z. Li, A novel disassembly process of end-of-life lithium-ion batteries enhanced by online sensing and machine learning techniques, J. Intell. Manuf. 34 (2023) 2463–2475, https://doi.org/10.1007/s10845-022-01936-x.
[57] L. Somerville, Post-mortem Analysis of Lithium-ion Cells After Accelerated Lifetime Testing, phdthesis, University of Warwick, 2017.
[58] Electrical resistances of soldered battery cell connections, J. Energy Storage 12 (2017) 45–54, https://doi.org/10.1016/j.est.2017.03.019.
[59] D.H. Doughty, E.P. Roth, A general discussion of Li ion battery safety, Electrochem. Soc. Interface 21 (2012) 37, https://doi.org/10.1149/2.F03122if.
[60] J.S. Gnanaraj, E. Zinigrad, L. Asraf, H.E. Gottlieb, M. Sprecher, M. Schmidt, W. Geissler, D. Aurbach, A detailed investigation of the thermal reactions of LiPF6 solution in organic carbonates using ARC and DSC, J. Electrochem. Soc. 150 (2003) A1533, https://doi.org/10.1149/1.1617301.
[61] T.T.D. Nguyen, Understanding and Modelling the Thermal Runaway of Li-ion Batteries, phdthesis, Université de Picardie Jules Verne, 2021, https://theses.hal.science/tel-03617656.
[62] X. Feng, M. Ouyang, X. Liu, L. Lu, Y. Xia, X. He, Thermal runaway mechanism of lithium ion battery for electric vehicles: a review, Energy Storage Mater. 10 (2018) 246–267, https://doi.org/10.1016/j.ensm.2017.05.013.
[63] H. Park, T. Yoon, J. Mun, J.H. Ryu, J.J. Kim, S.M. Oh, A comparative study on thermal stability of two solid electrolyte interphase (SEI) films on graphite negative electrode, J. Electrochem. Soc. 160 (2013) A1539, https://doi.org/10.1149/2.095309jes.
[64] Q. Wang, J. Sun, X. Yao, C. Chen, Thermal stability of LiPF6/EC+DEC electrolyte with charged electrodes for lithium ion batteries, Thermochim. Acta 437 (2005) 12–16, https://doi.org/10.1016/j.tca.2005.06.010.
[65] D.D. Agwu, F. Opara, N. Chukwuchekwa, D. Dike, L. Uzoechi, Review of Comparative Battery Energy Storage Systems (Bess) For Energy Storage Applications in Tropical Enviroments, 2018.
[66] A. Mosavi, F. Salehi, L. Nadai, S. Karoly, N.E. Gorji, Modeling the temperature distribution during laser hardening process, Results Phys. 16 (2020) 102883, https://doi.org/10.1016/j.rinp.2019.102883.

[67] H.A. Islava, Radial vs. Axial Cooling for 18650 lithium Ion Battery Cells - California State University, Sacramento, masterthesis, n.d. https://scholars.csus.edu/esploro/outputs/9925788849400167 1?institution=01CALS_USL&skipUsageReporting=true&recordUsage=false (accessed December 8, 2023).
[68] K. Ozawa, Lithium-ion rechargeable batteries with LiCoO2 and carbon electrodes: the LiCoO2/C system, Solid State Ionics 69 (1994) 212–221, https://doi.org/10.1016/0167-2738(94)90411-1.
[69] E.P. Roth, G. Nagasubramanian, Thermal stability of electrodes inLi-ion cells, Technical Report SAND2000-0345J, SandiaNational Laboratories, USA, 2000.
[70] D. Aurbach, B. Markovsky, A. Rodkin, M. Cojocaru, E. Levi, H.-J. Kim, An analysis of rechargeable lithium-ion batteries after prolonged cycling, Electrochim. Acta 47 (2002) 1899–1911, https://doi.org/10.1016/S0013-4686(02)00013-0.
[71] M. Spielbauer, J. Soellner, P. Berg, K. Koch, P. Keil, C. Rosenmüller, O. Bohlen, A. Jossen, Experimental investigation of the impact of mechanical deformation on aging, safety and electrical behavior of 18650 lithium-ion battery cells, J. Energy Storage 55 (2022) 105564, https://doi.org/10.1016/j.est.2022.105564.
[72] M. Spielbauer, P. Berg, M. Ringat, O. Bohlen, A. Jossen, Experimental study of the impedance behavior of 18650 lithium-ion battery cells under deforming mechanical abuse, J. Energy Storage 26 (2019) 101039, https://doi.org/10.1016/j.est.2019.101039.
[73] L.H.B. Nguyen, P.S. Camacho, J. Fondard, D. Carlier, L. Croguennec, M. R. Palacin, A. Ponrouch, C. Courrèges, R. Dedryvère, K. Trad, C. Jordy, S. Genies, Y. Reynier, L. Simonin, First 18650-format Na-ion cells aging investigation: a degradation mechanism study, J. Power Sources 529 (2022) 231253, https://doi.org/10.1016/j.jpowsour.2022.231253.
[74] A. Saidi, A. Tanguy, M. Fourmeau, G. Molnár, A. Boucherif, D. Machon, Coupling between mechanical stresses and lithium penetration in a lithium ion battery, Mech. Mater. 177 (2023) 104532, https://doi.org/10.1016/j.mechmat.2022.104532.
[75] L. Willenberg, P. Dechent, G. Fuchs, M. Teuber, M. Eckert, M. Graff, N. Kürten, D. U. Sauer, E. Figgemeier, The development of jelly roll deformation in 18650 lithium-ion batteries at low state of charge, J. Electrochem. Soc. 167 (2020) 120502, https://doi.org/10.1149/1945-7111/aba96d.
[76] W. Diao, B. Xu, M. Pecht, Charging induced electrode layer fracturing of 18650 lithium-ion batteries, J. Power Sources 484 (2021) 229260, https://doi.org/10.1016/j.jpowsour.2020.229260.
[77] B. Xu, L. Kong, G. Wen, M.G. Pecht, Protection devices in commercial 18650 lithium-ion batteries, IEEE Access 9 (2021) 66687–66695, https://doi.org/10.1109/ACCESS.2021.3075972.
[78] L. Willenberg, Volume Expansion and Its Effects on the Ageing of a Cylindrical Lithium-ion Battery, phdthesis, 2020.
[79] T. Waldmann, B.-I. Hogg, M. Wohlfahrt-Mehrens, Li plating as unwanted side reaction in commercial Li-ion cells – a review, J. Power Sources 384 (2018) 107–124, https://doi.org/10.1016/j.jpowsour.2018.02.063.
[80] T.-W. Wang, T. Liu, H. Sun, Direct recycling for advancing sustainable battery solutions, Mater. Today Energy 38 (2023) 101434, https://doi.org/10.1016/j.mtener.2023.101434.
[81] C. Fear, D. Juarez-Robles, J.A. Jeevarajan, P.P. Mukherjee, Elucidating copper dissolution phenomenon in Li-ion cells under overdischarge extremes, J. Electrochem. Soc. 165 (2018) A1639, https://doi.org/10.1149/2.0671809jes.
[82] N.K. Gada, Experimental and Theoretical Analysis of Safety-degradation Interaction in Lithium-ion Cells, masterthesis, https://core.ac.uk/reader/87262030, 2017. (Accessed 8 December 2023).
[83] M. Lewerenz, A. Warnecke, D.U. Sauer, Post-mortem Analysis on LiFePO4| Graphite Cells Describing the Evolution & Composition of Covering Layer on Anode and Their Impact on Cell Performance, phdthesis, https://linkinghub.elsevier.com/retrieve/pii/S0378775317313277, 2017. (Accessed 15 August 2023).
[84] J. Wilhelm, Diffraction Analysis of Anode Inhomogeneity in Lithium-ion Batteries, Technische Universität München, 2021. https://mediatum.ub.tum.de/1574633. (Accessed 8 December 2023).
[85] W. Ren, H. Chen, R. Qiao, Y. Lin, F. Pan, In-situ Probing of the Interfacial Kinetics for Studying the Electrochemical Properties of Active Particles and the State of Health of Li-ion Batteries, 2017.
[86] C. Fear, Overdischarge and External Short Behavior of Lithium-ion Batteries, Thesis, https://oaktrust.library.tamu.edu/handle/1969.1/177554, 2017. (Accessed 13 December 2023).
[87] D. Patel, Advanced Characterisation Techniques for Battery Safety Assessment, Doctoral, UCL (University College London), 2023, https://discovery.ucl.ac.uk/id/eprint/10172055/. (Accessed 13 December 2023).
[88] D.J. Robles, Degradation - Safety Analytics in Energy Storage, thesis, Purdue University Graduate School, 2019, https://doi.org/10.25394/PGS.9978782.v1.
[89] M.J. Lain, J. Brandon, E. Kendrick, Design strategies for high power vs. high energy lithium ion cells, Batteries 5 (2019) 64, https://doi.org/10.3390/batteries5040064.
[90] C.M. Jones, M. Sudarshan, R.E. García, V. Tomar, Direct measurement of internal temperatures of commercially-available 18650 lithium-ion batteries, Sci. Rep. 13 (2023) 14421, https://doi.org/10.1038/s41598-023-41718-w.
[91] Y. Guo, J. Cai, Y. Liao, J. Hu, X. Zhou, Insight into fast charging/discharging aging mechanism and degradation-safety analytics of 18650 lithium-ion batteries, J. Energy Storage 72 (2023) 108331, https://doi.org/10.1016/j.est.2023.108331.
[92] X. Lin, K. Khosravinia, X. Hu, J. Li, W. Lu, Lithium plating mechanism, detection, and mitigation in lithium-ion batteries, Prog. Energy Combust. Sci. 87 (2021) 100953, https://doi.org/10.1016/j.pecs.2021.100953.
[93] C.E. Hendricks, Failure Mechanisms in Overdischarged and Overcharged Lithium-ion Batteries, phdthesis, http://hdl.handle.net/1903/25178, 2019. (Accessed 8 December 2023).
[94] H. Wang, Aging and Direct Recycling of Cathode Active Materials in Commercial Li-ion Cell, thesis, Carnegie Mellon University, 2020, https://doi.org/10.1184/R1/13208279.v1.
[95] D. Krsmanovic, Development of a Property Forecast Tool for Flexible Compositions of Li-ion Batteries, Including Raw Material Availability and Price Forming, masterthesis, https://publica.fraunhofer.de/handle/publica/282805, 2019. (Accessed 8 December 2023).
[96] J. Hu, Y. Liao, J. Cai, Z. Wang, W. Zhang, X. Zhou, Insight into health deterioration induced by multi-cycle external short circuits in commercial 18650 lithium-ion battery, J. Electrochem. Soc. 168 (2021) 090565, https://doi.org/10.1149/1945-7111/ac2826.
[97] R. Carter, E.J. Klein, R.W. Atkinson, C.T. Love, Mechanical collapse as primary degradation mode in mandrel-free 18650 Li-ion cells operated at 0 °C, J. Power Sources 437 (2019) 226820, https://doi.org/10.1016/j.jpowsour.2019.226820.
[98] B.M. Huhman, A Single-frequency Impedance Diagnostic for State of Health Determination in Li-ion 4P1S Battery Packs, phdthesis, Virginia Tech, 2017, http://hdl.handle.net/10919/80573. (Accessed 13 December 2023).
[99] P. Iurilli, EIS applied to Li-ion Batteries: Modelling Cell Aging for Comprehensive SoH Estimation, Doctoral Thesis, ETH Zurich, 2022, https://doi.org/10.3929/ethz-b-000589948.
[100] T. Rauhala, K. Jalkanen, T. Romann, E. Lust, N. Omar, T. Kallio, Low-temperature aging mechanisms of commercial graphite/LiFePO4 cells cycled with a simulated electric vehicle load profile—a post-mortem study, J. Energy Storage 20 (2018) 344–356, https://doi.org/10.1016/j.est.2018.10.007.
[101] N. Al-Zubaidi R-Smith, M. Leitner, I. Alic, D. Toth, M. Kasper, M. Romio, Y. Surace, M. Jahn, F. Kienberger, A. Ebner, G. Gramse, Assessment of lithium ion battery ageing by combined impedance spectroscopy, functional microscopy and finite element modelling, J. Power Sources 512 (2021) 230459, https://doi.org/10.1016/j.jpowsour.2021.230459.
[102] G. Zhang, X. Wei, S. Chen, J. Zhu, G. Han, X. Tang, W. Hua, H. Dai, J. Ye, Comprehensive investigation of a slight overcharge on degradation and thermal runaway behavior of lithium-ion batteries, ACS Appl. Mater. Interfaces 13 (2021) 35054–35068, https://doi.org/10.1021/acsami.1c06029.
[103] B. Mao, C. Zhao, H. Chen, Q. Wang, J. Sun, Experimental and modeling analysis of jet flow and fire dynamics of 18650-type lithium-ion battery, Appl. Energy 281 (2021) 116054, https://doi.org/10.1016/j.apenergy.2020.116054.